Materials Today Bio 22 (2023) 100786

Contents lists available at ScienceDirect

Materials Today Bio

journal homepage: www.journals.elsevier.com/materials-today-bio

Extracellular matrix type 0: From ancient collagen lineage to a versatile product pipeline – JellaGel™

Nilofar Faruqui [a], David S. Williams [b], Andrea Briones [a], Ibolya E. Kepiro [a], Jascindra Ravi [a], Tristan O.C. Kwan [a], Andrew Mearns-Spragg [b], Maxim G. Ryadnov [a,*]

[a] National Physical Laboratory, Hampton Road, Teddington, TW11 0LW, UK
[b] Jellagen Ltd, Capital Business Park, Cardiff, CF3 2PX, UK

ARTICLE INFO

Keywords:
Extracellular matrix
Collagen
Organoids
Stem cells
Neural firing
Cell differentiation

ABSTRACT

Extracellular matrix type 0 is reported. The matrix is developed from a jellyfish collagen predating mammalian forms by over 0.5 billion years. With its ancient lineage, compositional simplicity, and resemblance to multiple collagen types, the matrix is referred to as the extracellular matrix type 0. Here we validate the matrix describing its physicochemical and biological properties and present it as a versatile, minimalist biomaterial underpinning a pipeline of commercialised products under the collective name of JellaGel™. We describe an extensive body of evidence for folding and assembly of the matrix in comparison to mammalian matrices, such as bovine collagen, and its use to support cell growth and development in comparison to known tissue-derived products, such as Matrigel™. We apply the matrix to co-culture human astrocytes and cortical neurons derived from induced pluripotent stem cells and visualise neuron firing synchronicity with correlations indicative of a homogenous extracellular material in contrast to the performance of heterogenous commercial matrices. We prove the ability of the matrix to induce spheroid formation and support the 3D culture of human immortalised, primary, and mesenchymal stem cells. We conclude that the matrix offers an optimal solution for systemic evaluations of cell-matrix biology. It effectively combines the exploitable properties of mammalian tissue extracts or top-down matrices, such as biocompatibility, with the advantages of synthetic or bottom-up matrices, such as compositional control, while avoiding the drawbacks of the two types, such as biological and design heterogeneity, thereby providing a unique bridging capability of a stem extracellular matrix.

Extracellular matrices (ECMs) provide a structural, mechanical and functional support for cell growth and tissue development [1]. They serve as substrate materials introducing biophysical cues that instruct tissue patterning with control over complex multicellular geometries [2,3]. ECMs are products of protein self-assembly – a hierarchical, non-covalent process which endows such matrices with responsiveness to external stimuli and positive tropism towards cell-induced processes such as matrix remodeling [4]. This unique role of the ECMs in creating and maintaining extracellular niches stimulates the development of ECM-like materials for biomedical applications [5]. To this effect, both top-down and bottom-up approaches have been devised. Top-down materials derive from decellularised tissues and find use in culturing tissue models, e.g., organoids [6–8]. Such materials are typically collagenous mammalian extracts, with Matrigel™ being a common example [9]. However, these materials are heterogenous in composition, lack detailed characterisation and may pose risks of transferring immuno- and pathogenic factors. To address these drawbacks, bottom-up alternatives have been proposed. These are artificial, synthetic matrices, which are generated using different chemistries and fabrication methods, including protein self-assembly, and tend to derive from fewer constituents than their native counterparts. This distinction renders bottom-up materials more suitable for systemic evaluations of the complex interplay between cells and their environment [10–14]. Synthetic analogues lack but can be functionalised with specialist biology, e.g., cell adhesion motifs [15–17], and their physical properties, e.g., stiffness and elasticity, can be tailored to meet the requirements of cell lineage specification [18,19]. Designs conducive to matrix mimetics successfully emulate protein fibril morphology providing compositional control, site specificity and nanoscale order [20–24], characteristic of native collagen fibres [25–27]. However, most of such designs fall short of replicating the topological complexity of the native ECM. These fibril structures lack network formation and porosity at the microscale [28,

* Corresponding author.
E-mail address: max.ryadnov@npl.co.uk (M.G. Ryadnov).

https://doi.org/10.1016/j.mtbio.2023.100786
Received 30 May 2023; Received in revised form 25 August 2023; Accepted 28 August 2023
Available online 29 August 2023
2590-0064/© 2023 The Authors. Published by Elsevier Ltd. This is an open access article under the CC BY-NC-ND license (http://creativecommons.org/licenses/by-nc-nd/4.0/).

29]. Although it is possible to exert control over the morphology of these fibrils and programme them into polygonal fibrous networks [30,31], even reaching appreciable porosity at the microscale [32], the level of predictability achieved in these synthetic designs remains insufficient to fully replicate the ECM.

Thus, top-down materials appear complex and heterogeneous in composition to support systemic evaluations of cell-matrix biology, whereas bottom-up matrices require biofunctionalization and improved predictability in design. A material, which combines the biological origin of top-down matrices with the minimalist compositional control of synthetic designs, may provide an optimal solution.

With over 28 different collagen types identified in mammalian tissues [33], only a few are essential for matrix formation, whilst each type has a specific functional role. Such specialisation supports the complexity of mammalian physiology, which underpins the diversity of mammalian collagens, but also suggests the existence of a non-mammalian precursor type. Indeed, the collagen matrix from jellyfish shares similarities in chemical composition with different, rather than one, collagen types yet predating them all by around 0.6 billion years [34,35]. Therefore, this matrix can be viewed as a stem of all collagen matrices: a precursor for all the matrices of higher animals. Although this matrix exhibits essential fibrillar properties of other collagen matrices, e.g., collagen type I, and can be considered as collagen type I-like [36], it demonstrates unique behaviours and amino-acid fingerprints reflective of its undifferentiated, evolutionary primitive form which precedes type I [34–36]. Without belonging to one particular type and due to its ancient biochemical lineage, compositional simplicity, and resemblance to multiple collagen types (e.g., I, II, III, V, IX), this matrix lends itself as a matrix type 0 [34–41]. It may be plausible that there has been a non-collagenous matrix, which may predate this one, but has yet to be discovered. Therefore, for the purpose of this report, which focuses on collagen based ECMs we refer to this matrix as a collagen matrix type 0. This type offers an advanced material that has been tested, optimized, and validated over millions of years. Surprisingly, however, there is scarce information as to the physical and biological properties of the type beyond two-dimensional (2D) cell adhesion studies [42,43], and research efforts using three-dimensional (3D) sponge scaffolds derived from re-fibrillised and lyophilised mesoglea [44–46]. Similar to other prefabricated top-down extracts, mesoglea scaffolds can be utilised as effective niche substrates to harness endogenous regenerative mechanisms. However, these scaffolds are heterogenous, and their sponge forms restrict the spatial organisation of tissues. For some tissues, e.g., bone or cartilage, spatial restriction may be beneficial, but other, structurally anisotropic, tissues exhibit more profound dependence on matrix re-alignment and re-modelling [47–49]. Sol-gel matrices which may better mimic the plasticity of the native ECM are of increasing demand, whereas a matrix assembled in aqueous solution from a purified collagen type 0 encapsulating live cells has yet to be shown. Herein we introduce such a matrix and provide its functional profile in 2D and 3D cell culture. We refer to it as an extracellular matrix type 0.

1. Results and discussion

1.1. Matrix origin, morphology and folding

The matrix used in the study originates from *R. pulmo*. The material was developed following a proprietary manufacturing process established by Jellagen Ltd. The process combines an acid extraction with downstream purification to yield a purified material to Jellagen internal specifications (Fig. 1A). The material, namely JellaGel™, is then set at the laboratory scale for physicochemical and, with cells, biological assessments (Fig. 1B). The physicochemical properties of the resultant material were characteristic of fibrillar collagens. Transmission electron microscopy (TEM) of JellaGelTM preparations revealed networks of extended fibres 10s of microns in length (Fig. 1C). Individual fibres had an average diameter of 23 ± 2 nm and appeared as protofibril bundles (Fig. 1D). Although this is consistent with the packing modes of collagen types I and II [50], only a fraction of these fibres was D-periodic (Fig. 1E). The observed periodicity was at the expected value of 67–68 nm and D-periodic fibres were 10-nm thicker suggesting that the maturation of the fibres was delayed or arrested in these preparations [26]. Instead, most fibres had an appreciable pattern of longitudinal striations commonly found in orderly helical fibres whose protofilaments run parallel to the fibre axis (Fig. 1D) [51,52]. The lack of the D-periodicity in the fibres may manifest in the high structural flexibility of the jellyfish collagen rendering it permissive to extensive fibre networks. Indeed, intricate networks of high fibre densities were more characteristic for these preparations than persistent individual fibres. The relative homogeneity of the fibres in the networks observed by TEM was found to be consistent with that no aggregation was detected for the material by Dynamic Light Scattering (DLS). Hydrodynamic diameters for JellaGel™ proved to be stable over a month within the range of 80–216 nm, with no partitioning observed towards bigger sizes (Fig. 2A & S1 in Supporting Information). This tendency remained consistent with high intercepts in DLS correlograms recorded for JellaGelTM samples upon dilution. By contrast, broad ranges of hydrodynamic diameters were observed for bovine collagen type I (BCTI) used as a fibrillar material of mammalian origin for comparison. These were 100 times larger than the 20–500 nm range typically assigned to collagen

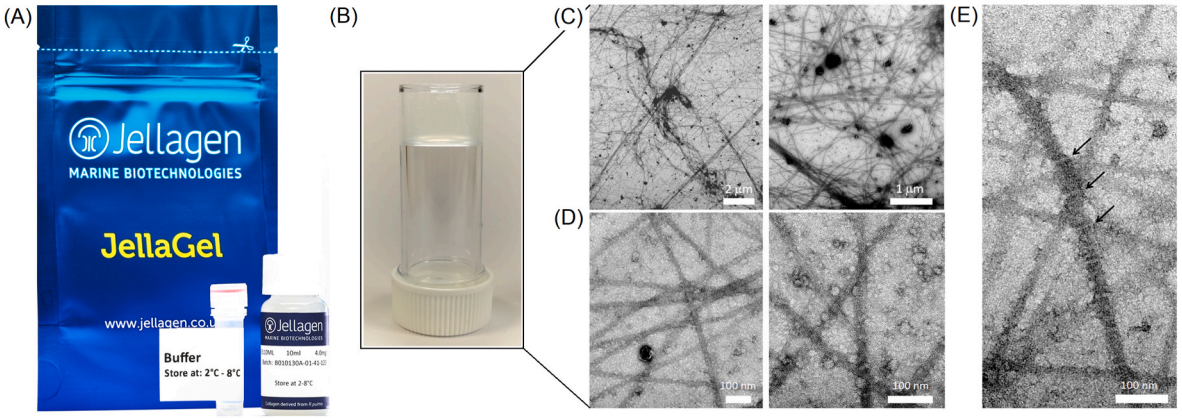

Fig. 1. Matrix origin and morphology. Photographs of the JellaGelTM kit (A) and gel set in a 5-mL vial (B) used for physicochemical and biological analyses. Low (C) and higher magnification (D) electron micrographs of high-density intricate networks of JellaGel™, with an apparent longitudinal striation pattern for individual fibres (D). (E) A collagen fibre with characteristic D-periodic bands of 67–68 nm between lighter axial striations highlighted by black arrows. Key: 1 g/L (total protein) in 10 mM phosphate buffered saline (PBS), pH 7.4.

fibres (Fig. 2A & S1) [53]. Furthermore, increasing dilutions led to low intercepts in the correlograms recorded for BCTI, but not for JellaGelTM (Fig. S1). This indicates multiple scattering in BCTI samples reflecting increased heterogeneity and instability in the assembly of this collagen matrix.

Circular Dichroism (CD) spectroscopy measurements of JellaGel™ preparations revealed the formation of an appreciable polyproline II helix, with spectral bands shifted towards lower wavelengths at 215–220 nm (positive) and 195–200 nm (negative) (Fig. 2B). This is in comparison to a typical polyproline II helix exhibiting positive and negative bands at around 228 nm (n-π^* transition) and 206 nm (π-π^* transition), respectively [54]. The effect is common for collagen sequences incorporating polar and charged residues and results from differences in transition energies between tertiary, secondary and primary

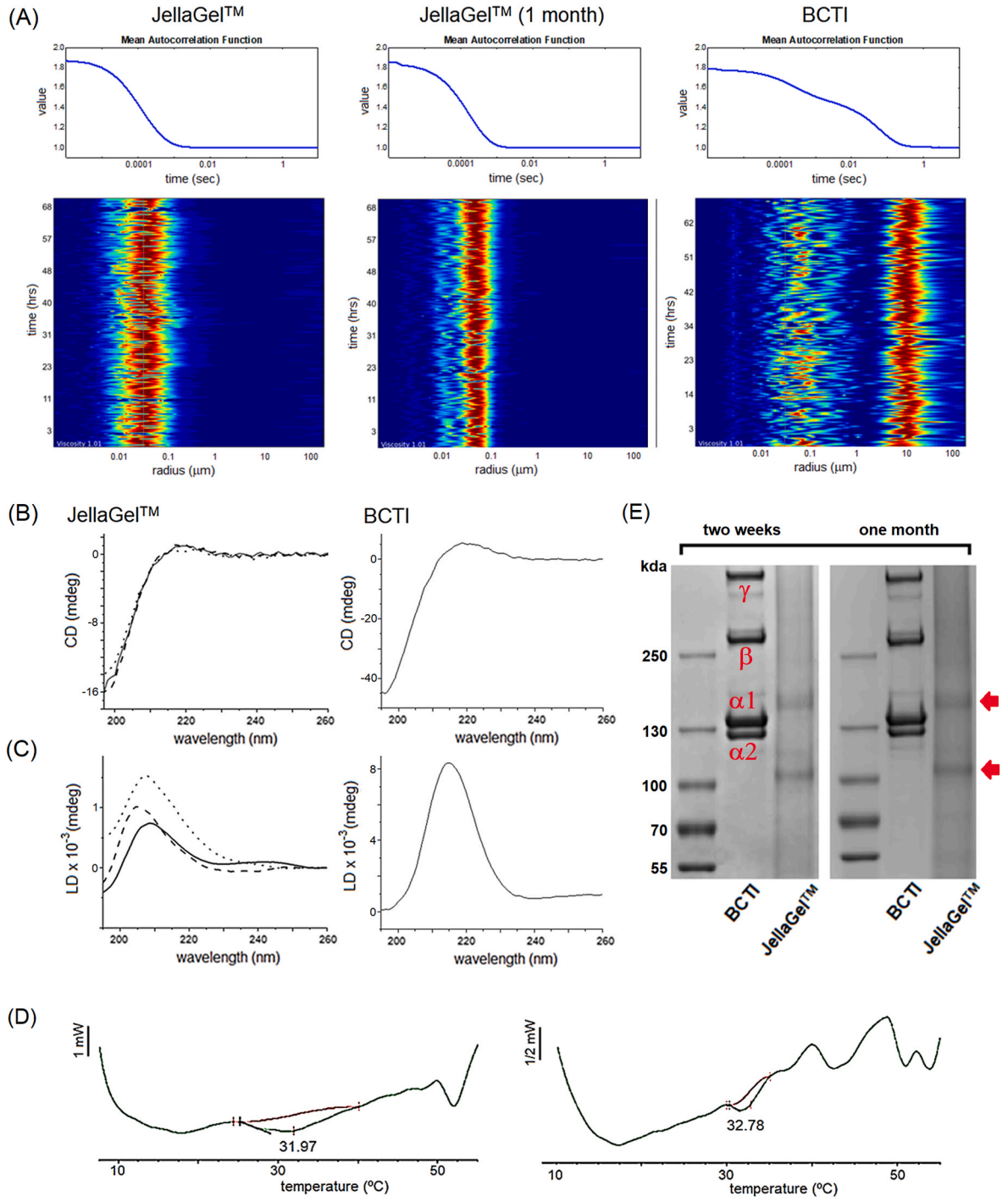

Fig. 2. Matrix folding and stability. (A) DLS traces for JellaGelTM and BCTI recorded for two-fold dilutions of stock preparations (1 g/L) continuously over three days. CD (B) and LD (C) spectra recorded for JellaGel™ (left) and BCTI (right). Key: 1 g/L and 0.1 g/L (total protein) for (B) and (C), respectively, in 10 mM PBS, pH 7.4. Dashed and dotted lines are for spectra recorded after maturation over two and three weeks, respectively. (D) DSC traces for JellaGel™ at 8 g/L (total protein) in 10 mM PBS (pH 7.4). Two different preparations are given to show variation ranges in transition temperatures. (E) SDS-PAGE electropherograms for JellaGel™ and BCTI recorded following maturation over two weeks and one month. The double-band patterns of JellaGel™ are labelled with red arrows, and BCTI chains are α1, α2, β and μ are labelled accordingly. (For interpretation of the references to colour in this figure legend, the reader is referred to the Web version of this article.)

amides [54,55]. Similar spectra were recorded for BCTI confirming close conformational similarities with jellyfish collagen (Fig. 2B). Linear Dichroism (LD) spectroscopy gave complementary evidence (Fig. 2C). LD signals reflect the difference in absorbance of linearly polarised light parallel and perpendicular to an orientation direction, which can be positive for transitions polarised along the direction and negative for transitions perpendicular to the direction [56]. Therefore, LD can reveal the orientation of secondary structure elements in the fibre with respect to its axis. LD spectra for JellaGel™ showed a single maximum at 206–208 nm (Fig. 2C). This signal requires a transition polarised along the axis at ~206 nm, and hence indicates that polyproline II helices in jellyfish collagen are aligned parallel to the fibre axis [57]. LD signals for BCTI were recorded at slightly higher wavelengths (215 nm), which may be attributed to the presence of larger assemblies as found by DLS. The CD and LD data showed no apparent changes in folding over a month, which is consistent with the DLS results over the same period of time (Fig. 2A–C).

Further, thermal denaturation experiments confirmed that the jellyfish collagen folded cooperatively (Fig. S2). Unlike BCTI, whose structure underwent an evident transition at 35 °C without regaining the original structure (Fig S2A), the loss of structure for the jellyfish collagen was more gradual and reversible (Fig S2B). Importantly, comparable spectra were recorded before and after the denaturation indicating that JellaGel™ maintained its structural integrity in response to heating up to 90 °C. The CD spectra suggest a likely transition midpoint at ~30-35 °C. Differential scanning calorimetry (DSC) measurements confirmed the transition at this temperature range (32-33 °C) and showed transitions at higher temperature ranges (40-53 °C) preceded by damping maxima peaks corresponding to exothermic reactions due to crystallisation (Fig. 2D). Collagens are typically resistant to heat and undergo irreversible denaturation at temperatures exceeding 40 °C, often via several stages of denaturation with secondary denaturation temperatures observed at higher temperature ranges (>50 °C) [58–61]. Thus, the cooperative folding of JellaGel™ and its thermal reversibility in the 5-90 °C range proves to be consistent with the re-assembly of the material in response to changing temperatures without complete denaturation.

Analyses by sodium dodecyl sulphate polyacrylamide gel electrophoresis (SDS-PAGE) and mass spectrometry provided further insight into the compositional stability of JellaGel™. A distinctive double band pattern of two major masses was observed by SDS-PAGE at ~115 kDa and 160 kDa (Fig. 2E). The pattern could be attributed to main polypeptides chains in jellyfish collagens [42,62,63]. In comparison, the expected pattern of higher masses equivalent to γ, β, α1 and α2 chains was found for BCTI.

The double band pattern for JellaGel™ appeared to be stable over a month, in accord with the results obtained by the light scattering and spectroscopy measurements. Mass spectrometry confirmed the mass ranges for both collagens, suggesting that the jellyfish collagen is formed by a polypeptide chain of 160 kDa, equivalent to the β isomer of BCTI, and a compositional constituent of 110–115 kDa without a dominating mass akin to that of α1 and α2 chains in BCTI (Fig. S3A). *In silico* peptide fingerprinting analysis performed against existing protein databases revealed close matches in peptide fragmentation patterns for BCTI and human type I, II, III and V collagens. All these collagens shared similar fragment counts in the same mass range. All had comparably low abundances in the lower part of m/z 500–1000, and similar patterns of decreasing counts in m/z 1000–7000 (Fig. S3B). Notably, counts at m/z 1000 were prevalent for all these collagens. In marked contrast, fragment counts for JellaGel™ were negligible for the low range, including those at m/z 1000, and exhibited comparable counts at m/z 2000–6000 – the pattern that was distinct from those observed for the other collagens. These findings indicate that the primary structure composition of JellaGel™ is different from those of mammalian collagens.

Collectively, the biophysical data indicates that the material forms high-density networks of discrete fibres of conserved morphology and high compositional stability.

1.2. Functional support for cell networking, polarity, and synchronicity

Fibre network formation is pre-requisite for supporting specialised functions. Of particular importance, this is for asymmetric types of cell organisation, such as the unidirectional transmission of electric signals in neurons. To probe JellaGel™ as a compatible substrate for functional cell networking, the comparative evaluation of the material was performed to co-culture astrocytes and cortical neurons.

Apart from viability and proliferation, which are common requirements for most cell models, cell polarity, networking and synchronicity are critical factors for nervous systems to function. A suitable ECM is required to form persistent networks that can support the intricacy of cell networks over relevant time and length scales. The co-culture of astrocytes and neurons presents an optimal asymmetric model to probe functionality of fibre networks without the complexity of bulk matrix properties such as gelation, cell encapsulation and tensile strength. To allow comparison Matrigel™ was used as a top-down matrix control. Both materials supported the growth of astrocytes derived from human induced pluripotent stem cells (iPSCs) – BIONi010–C. Immunocytochemistry experiments revealed the quantitative growth of viable cells for both substrates over four days (Fig. S4A). Similarly, co-cultures of astrocytes plated on the substrates with cortical neurons, derived from the same iPSCs, effectively formed viable neuronal networks over a week of incubation on both substrates (Fig. 3A & S4B). Variations between the two matrix materials occurred at different maturation times of BIONi010–C astrocytes. The astrocytes were incubated on either substrate over one or seven days before plating BIONi010–C neurons for a further seven days in culture. The neuronal adherence was comparable under every condition used, whereas neurite outgrowth was more appreciable on Matrigel™ for astrocytes matured for one day (Fig 3A & S4C). This may be explained by the fact that the matrix is not a purified ECM, is rich in growth factors and matrix proteins which accelerate cell growth. The cell networks on Matrigel™ appeared to be denser and spatially less defined than those on JellaGel™, which may also result from that the collagen of Matrigel™ is heterogeneous and like BCTI is prone to aggregation (Fig S4B, C). The patterns of cell networks for each matrix proved to be reproducible for different cell densities (0.5-2 x 10^5 per cm^2) and were independent of mitotic inhibitors (Fig S4B, C). Given that cultures based on the astrocytes matured over seven days were similar for both matrices, these conditions were selected to evaluate neuron firing synchronicity using spontaneous neural activity assays. The assays make use of a lentiviral reagent (Incucyte® Neuroburst Orange Lentivirus) to promote the expression of a genetically encoded orange fluorescent (mRuby) in neuronal cells. The reagent allows for the non-disruptive labelling of neurons over several days or weeks to quantify the functional connectivity of neuronal networks. After four days of co-culturing, the reagent was titrated into the cells. Regular scans over 22 days post-transfection were performed to compare the counts of active cells (active counts), synchronisation of the cells (network correlations) and the average number of bursts per neuron per min (burst frequency) (Fig. S5). Higher neuron numbers exhibiting higher burst frequencies were observed for Matrigel™ (Figs. S5A and B). Strikingly, the mean correlations of functional connectivity in cell networks were higher on JellaGel™ than on Matrigel™, 0.95 versus 0.75, respectively (Fig. S5C). The value did not change for JellaGel™ when supplemented with laminin at the molar ratio of 80/20% (Fig. S6A). This can be expected despite that higher numbers of active cells with high burst frequencies were observed for the laminin preparation (Figs. S6B and C). Indeed, neuronal network correlations should not depend on the number of active cells. Correlations relate to the tuning similarity of two neurons to stimuli and the degree of fluctuations in response strength shared by the two neurons [64]. Responses can correlate at different time scales but exhibit redundancy when summed over a cluster of cells, while being

independent of the cluster size [65]. With the repeated presentation of identical stimuli to the matrices used in this study, the differences in the correlations observed are likely to relate to co-fluctuations in responses of neuron subsets as opposed to fluctuations for all cells. Given that laminin does not assemble or co-assemble with collagen, variability implications due to structural changes of the matrix can be excluded. Therefore, the results suggest that it is the network composition of JellaGel™ that is primarily responsible for the observed correlations. Further support for this came from the kinetic measurements of neuron connectivity for Matrigel™ and JellaGel™, with both showing strong burst synchronicity (Fig. 3B and C).

Matrigel™ supported higher burst intensities. Interestingly, split spike responses were apparent for this matrix as well, which is likely to reflect on its compositional and structural heterogeneity (Fig. 3B and Video S1, Supporting Information). High levels of background noise were also evident. In marked contrast, appreciable single spike responses of lower intensities with much lower levels of background noise were recorded for JellaGel™, which also supported spatially extended networks of firing neurons (Fig. 3B and Video S2). Collectively, these findings indicate that JellaGel™ effectively promotes the formation and functional synchronicity of human neuronal networks.

Supplementary video related to this article can be found at doi:10.1016/j.mtbio.2023.100786

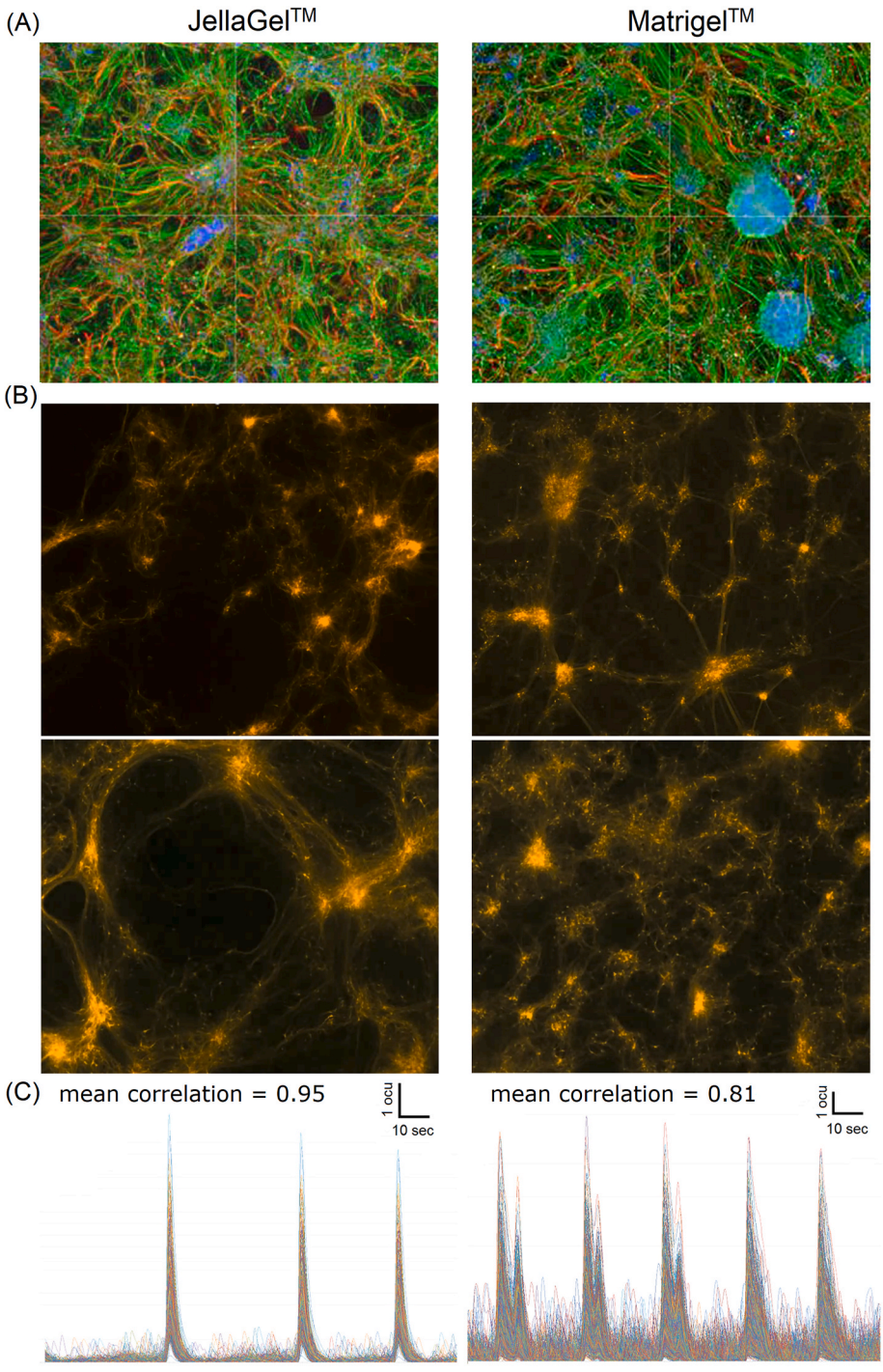

Fig. 3. Matrix support for neuronal networks. (A) Fluorescence micrographs of co-cultured astrocytes and neurons derived from BIONi010–C iPSCs taken at 20x magnification. Astrocytes plated on substrates at a seeding density of $10^5/cm^2$ and matured over seven days before adding neurons. After further seven days of culture the plates were fixed and stained with markers for neurons (green, TuJ1 - class III beta-tubulin), astrocytes (red, Glial fibrillary acidic protein (GFAP) and nuclei (blue, Hoechst 33342). (B) Neuron firing synchronicity at 20x magnification on Matrigel™ *and* JellaGel™ and (C) corresponding correlation diagrams (C). See also representative Videos S1 and S2, Supporting Information. (For interpretation of the references to colour in this figure legend, the reader is referred to the Web version of this article.)

1.3. Matrix support in 3D: immortalised, primary and stem cells

The ability of JellaGelTM to support 3D cell culture versus that of Matrigel™ was assessed across different human cell types including immortalised (cervical carcinoma, HeLa; osteosarcoma, MG-63), primary (human dermal fibroblasts; osteoblasts), and human mesenchymal stem cells (hMSCs). Fluorescence microscopy analyses revealed progressive cell colonization over time in JellaGel™ and Matrigel™ hydrogels, consistent with cell proliferation rates measured using PrestoBlue® cell proliferation assays (Fig. 4A, B, S7 & S8). Comparable cell counts and proliferation rates at set time points over seven days of incubation were observed for the two matrices, with variations being within an experimental error in all cases (Figs. S7 and S8). These findings indicate that JellaGel™ effectively supports 3D culture independent of the cell type used.

No apparent differences were observed in the morphology of cells encapsulated in JellaGel™ and Matrigel™. Immortalised and primary cells assumed round shapes, which were in contrast to spread morphologies observed for the same types of cells grown on the matrices used as 2D coatings. In 2D, the matrices are stiff substrates restricting cell adhesion to one plane while promoting cell polarity, as was shown for the neurite outgrowth. As a consequence, adherent cells are expected to spread on the substrates. When used as gels, the matrices provide soft substrates promoting adhesion in 3D, which hinders cell spreading and polarity [3,19]. The behaviour of immortalised and primary cells used in the study was fully consistent with the differences outlined (Figs. S7 and S8). Intriguingly, MSCs used at the same cell densities as the other cell types appeared to spread in 3D (Fig. 4A). MSCs rely on enhanced paracrine communication to build up sufficient cellular tension to differentiate, which is also linked to profound dependence of MSCs on matrix stiffness [66,67]. In 2D matrices, many adhesive ligands are readily accessible, whereas in 3D cells have to reach out to and gather such ligands, which prompts the formation of lamellipodial extensions and cell spreading and networking [67].

Further, immortalised cells were found to favour cell-to-cell interactions resulting in cell clustering in both matrices. This effect may be expected as immortalised cells readily aggregate, likely to mitigate the lack of accessible adhesion ligands in 3D. The cells also have no preference for lamellipodia or bleb extensions and employ low-adhesion motility modes, e.g., by adopting amoeba-like morphologies [68,69].

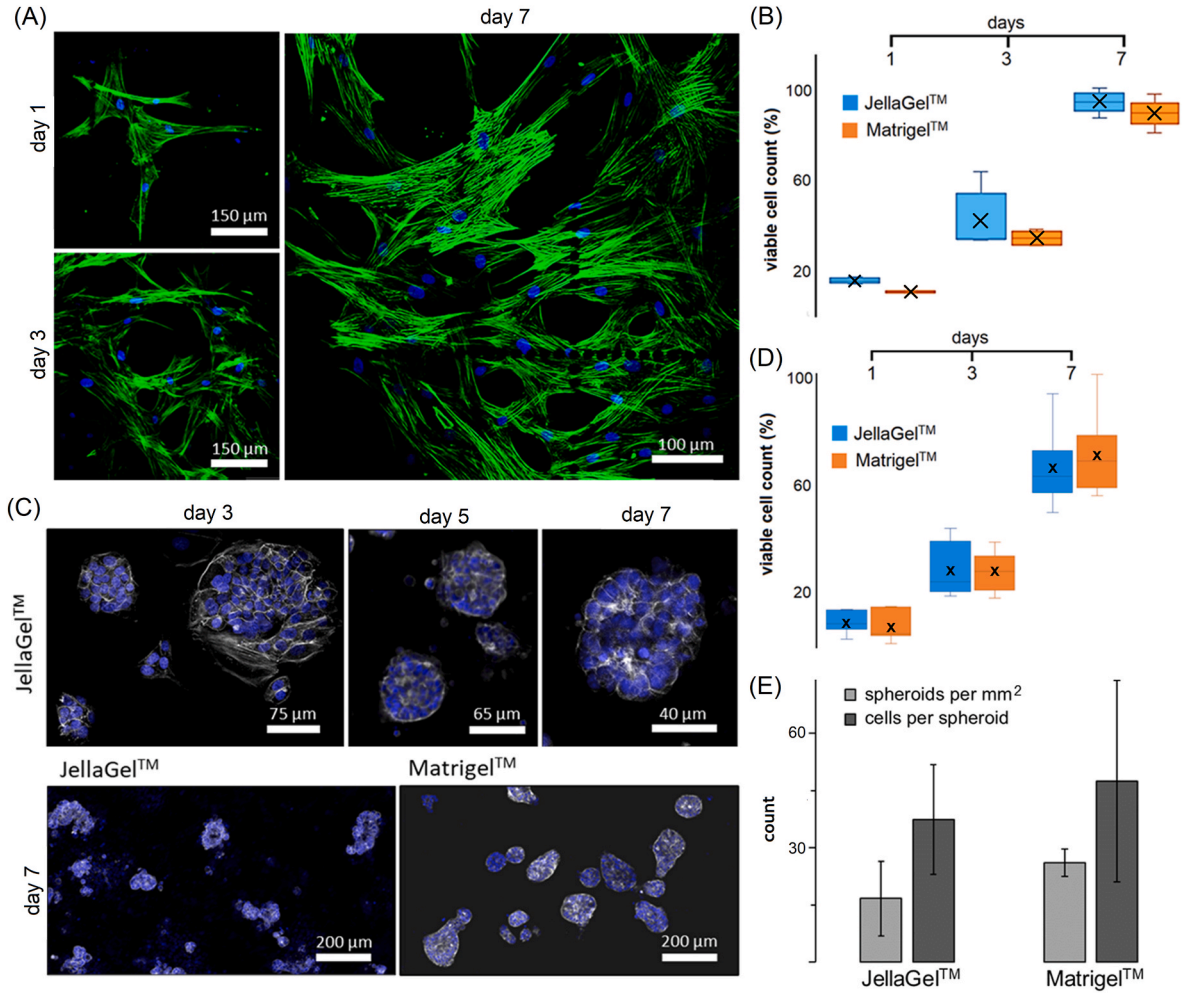

Fig. 4. Matrix support in 3D and spheroid formation. (A) Fluorescence micrographs of hMSCs in JellaGel™. The cells were stained with Alexa Fluor® conjugated phalloidin to stain actin (green), and Hoechst 33342 to stain nuclei (blue). Cell seeding density is 4×10^5 cells/mL. (B) Boxplots of total viable counts of hMSCs by PrestoBlue® assays as a function of time showing the mean (x), median (horizontal line in the box), 25th percentile (bottom edge of the box), 75th percentile (top edge). Total number of hMSCs in JellaGel™ on day 7 is taken as 100%. (C) Fluorescence micrographs of Michigan Cancer Foundation-7 (MCF7) cells stained with Alexa Fluor® conjugated phalloidin to stain actin (grey), and Hoechst 33342 to stain nuclei (blue). Cell seeding density is 4×10^5 cells/mL. (D) Boxplots of total viable counts of MCF7 cells by PrestoBlue® assays as a function of time showing the mean (x), median (horizontal line in the box), 25th percentile (bottom edge of the box), 75th percentile (top edge). Total number of cells in Matrigel™ on day 7 is taken as 100%. (E) Number of spheroids (counts) per unit area (mm^2) and number of cells per spheroid for MCF7 grown in both matrices on day 7 of incubations. Note: the perforation line in some images is from the size grids used during imaging. (For interpretation of the references to colour in this figure legend, the reader is referred to the Web version of this article.)

Therefore, cell clustering is commonly exploited to produce spheroid and organoid structures, including the use of Matrigel™ [70,71].

To better understand if the matrices can seed spheroid formation, an established cell line for spheroid models was used [72]. Michigan Cancer Foundation-7 (MCF7) cells encapsulated in both JellaGel™ and Matrigel™ effectively formed spheroids over several days of incubation. With similar proliferation rates in both matrices, the cells appeared to give compact spheroids of round morphologies which tended to marginally grow both in size and numbers within a week (Fig. 4C–E and S9A, B). Dominating spheroid morphologies were estimated to comprise up to 100 cells per spheroid, with lager spheroids constituting a fraction of these, which proportionally increased over time (Fig. 4E and S9C). The spheroid formation, timescale, and size distribution, were comparable to those observed by others, confirming JellaGel™ as an effective matrix for generating spheroids [72-75].

2. Conclusion

We have described an extracellular collagen matrix that is derived from an evolutionary ancient collagen lineage, namely jellyfish collagens, which predate animal collagens while sharing similarities with them. We experimentally validated the physicochemical and functional attributes of this matrix with an emphasis on biological applications. We demonstrated that the matrix promoted the co-culture of human astrocytes and cortical neurons derived from iPSCs, effectively maintained spontaneous neural activity with correlations indicative of a homogenous extracellular material, which was in contrast to heterogeneous tissue-extract matrices (i.e., Matrigel™), supported the 3D culture of immortalised, primary and stem cells and induced appreciable spheroid formation.

Based on the results, we conclude that the matrix offers an optimal solution for systemic evaluations of cell-matrix biology and constitutes a versatile material that effectively combines mammalian tissue extracts, such as their biological origin, with those of synthetic designs, or bottom-up matrices, such as their minimalist compositional control, while avoiding the disadvantages of the two types, such as heterogeneity and poor biofunctionalization, respectively, thus providing a unique bridging capability of a stem extracellular matrix.

This study underpins the successful implementation of this advanced material as a high-value product, which has been commercialised under the proprietary name of JellaGel™. The material is devoid of drawbacks characteristic of the current commercial products, reflecting its simplicity and versatility as a likely originator of more complex matrices from higher animals. Most of existing commercial products rely on mammalian collagen type I, such as heterogeneous BCTI used in the study, which can also be of foetal origin, cellulosic materials, which are not biodegradable and require an additional means for degradation, such as the use of cellulase [76], sarcoma derived products such as Matrigel™, which promote metastasis and angiogenesis [77,78], or materials that can only be produced chemically and are amyloid-like [79]. JellaGel™ supports more homogeneous and uniform cell responses, it is devoid of mRNA, being a typical impurity of mammalian matrices [41], is biodegradable and does not rely on chemistry. Owing to such properties, the product is being applied in different areas including research and clinic proving the application versatility of the material as a stem of all collagens [80].

3. Experimental section

3.1. Materials

JellaGel™ was from Jellagen (UK) and prepared as per internal specifications. All materials were used as per suppliers' protocols. Bovine collagen type I was purchased from Gibco (Fisher Scientific, UK). Matrigel™ was purchased from Corning Inc. (USA). Incucyte® Neuroburst Orange Lentivirus reagent was from Sartorius (UK). Laminin, uridine, 5-fluro-2-deoxyuridine were purchased from Sigma. Cell lines were purchased from American Type Culture Collection (ATCC, UK): HeLa (CCL-2), MCF7 (ATCC HTB-22), MG-63 (CRL-185), A549 (CCL-185), hMSC (PCS-500-012); BIONi010–C iPSCs were from European Collection of Authenticated cell Cultures; human dermal fibroblasts were from Sigma-Aldrich (UK), and human osteoblast were from PromoCell (Germany).

3.2. Circular dichroism spectroscopy

CD spectra were obtained on a JASCO J-810 spectropolarimeter equipped with a Peltier temperature controller in a quartz cuvette with 0.05 cm pathlength. All measurements were taken in millidegrees using 1 nm step, 1 nm bandwidth, 1 s time/point and four acquisitions. Aqueous collagen solutions (300 μL, 1 g/L total protein, unless stated otherwise) were prepared in filtered (0.22 μm) 10 mM PBS, pH 7.4, at room temperature. CD spectra at variable temperatures were recorded with a 5 °C step from 5 to 90 °C with 180 s equilibration time for each spectrum.

3.3. Linear dichroism spectroscopy

Solution-phase flow LD spectroscopy was performed on a Jasco-810 spectropolarimeter using a photo elastic modulator 1/2 wave plate. A micro-volume quartz Couette flow cell featuring ~0.5 mm annular gap, and quartz capillaries were used (all from Kromatec Ltd, UK). Molecular alignment was done by applying the constant flow of the sample solution between two coaxial cylinders, a stationary quartz rod and a rotating cylindrical capillary. LD spectra were recorded with laminar flow achieved by maintaining the rotation speed at 3000 rpm and processed after subtracting non-rotating baseline spectra.

3.4. Dynamic light scattering

Measurements were performed *in situ* in a SpectroLight 610 instrument (Xtal Concepts GmbH, Germany) using Terasaki plates allowing for the simultaneous measurement of multiple samples as a function of time. JellaGelTM and BCTI samples were prepared in serial dilutions (1 x PBS) and were centrifuged (10,000×*g*, 10 min, 4 °C) to ensure that dust and other particulates are removed to prevent false positives. Each sample (2 μL) was loaded onto a Terasaki plate covered in paraffin oil to prevent evaporation. The sample were then measured over 68 h at 20 °C. The data was processed automatically using the proprietary software.

3.5. Differential scanning calorimetry

DSC experiments were carried out in the temperature range of 15–90 °C on a DSC-Q2000 instrument from TA Instruments. Collagen samples (in duplicate) at ~ 8 mg/mL in 10 mM PBS (pH 7.4) were placed in sealed crucibles along with the buffer alone as a reference sample. The heating rate was at 1 °C/min. The data was analysed using the TA Q-series Advantage Universal Analysis software and plotted using Origin software V7 (OriginLab).

3.6. Transmission electron microscopy

Droplets of collagen solutions, prepared as per Jellagen's specifications and diluted with PBS (x5), were placed on glow-discharged Cu grids coated with carbon film (EM Resolutions Ltd, UK). After 30 s, the excess solvent was removed by blotting with a filter paper. The grids were then passed over deionised water (two drops) to remove buffer salts and stained with phosphotungstic acid (aq. 4%, pH 7), followed by blotting the excess stain and allowing the grids to air dry. Electron micrographs were recorded in a Tecnai G2 transmission electron microscope (Thermo Fisher Scientific Inc., USA) operated at 200 keV using a 20-μm objective aperture to improve contrast. Images were taken using

an ORCA-HR CCD camera (Advanced Microscopy Techniques Corp, Danvers, USA).

3.7. Sodium dodecyl sulphate polyacrylamide gel electrophoresis

The 2 μL of the prepared JellaGel™ and BCTI solutions (1 mg/mL) were diluted using 13 μL of ultrapure water (Sigma, UK) and 5 μL of SDS-PAGE protein loading buffer (Thermo Scientific, UK). The samples were then heated to 90 °C for 5 min and electrophoresed in a 3–8% Tris-acetate gel, running buffer (1 x) in a BioRad cell device. Thermo Scientific™ PageRuler™ Plus Prestained Protein Ladder (ID 11852124) was used as a ladder of sizes from 10 to 250 kDa as shown in Fig. 2E. Coomassie brilliant blue was used to stain protein bands and identify their corresponding molecular masses against pre-stained protein ladders (Thermo Scientific, UK). The staining solution of Coomassie blue was prepared by dissolving Coomassie R250 (1 g) in methanol (300 mL) followed up by adding deionised water (650 mL) and acetic acid (50 mL). The prepared staining buffer (100 mL) was added to the gel and warmed up in the microwave before incubating in an orbital 3D shaker for 15 min at room temperature. The gel was rinsed in deionised water and let to distain overnight before imaging.

3.8. In silico trypsinisation

Expasy (https://web.expasy.org/peptide_mass/) was used to generate theoretical peptide masses of human collagen types I-III, V and BCTI (as per 07/02/2023). The protein sequences with entry numbers P02452, P02458, P02461, P25940 and P02769 were retrieved from UniProt.

3.9. Mass spectrometry analysis

JellaGel™ and BCTI samples were digested and processed using a trypsin singles, proteomic grade kit (Sigma Aldrich, UK) as per the manufacturer's protocol. 50 μL of protein was added to a 1:20 ratio of protein to trypsin. 49 μL of the trypsin reaction buffer was added to each vial to a final concentration of 20 mM. Reaction was vortexed and incubated overnight at 37 °C.

Spectra of undigested samples were manually acquired in an Autoflex III TOF/TOF mass spectrometer using FlexControl software (version 3.0) (Bruker Daltonik, GmbH). Equal volumes of protein calibration standard I and peptide calibration standard were used (both from Bruker Daltonik, Germany). The mixture (13 molecules) was used as an internal calibrant as per the manufacturer's instructions. Samples were mixed (1:3) with α-cyano 4-hydroxycinnamic acid (CHCA) (Agilent, UK) used as a matrix and spotted (1 μL) in triplicates onto an MTP 384 target plate ground (Bruker Daltonik, Germany). Spectra of digested samples were acquired in a matrix-assisted laser desorption/ionization (MALDI) mass spectrometer (SYNAPT G2-Si, from Waters, USA) equipped with a resolving quadrupole and dual-collision TriWave. All mass spectra were recorded in a positive mode with a mass resolution of ~14000 (fwhm). The data were acquired by irradiating each pixel with 250 (Nd:YAG laser) or 60 pulses (N2 laser). Mass calibration was performed using red phosphorus cluster ions (Sigma-Aldrich, UK) and samples were mixed with CHCA as described above.

3.10. 2D cell culture and coating

JellaGel™ (Jellagen, UK) and growth factor reduced Matrigel™ (Corning, UK) solutions were prepared as per the manufacturers' protocols. Matrigel™ (2 mg) was diluted in 9 mL of cold Dulbecco Minimal Essential Eagle's Medium (DMEM) supplemented with Ham's nutrient mixture F-12 (ThermoFisher, UK). 100 μL of the solution was added to each well of a TPP 96-well plate, which was then incubated for 1 h at 37 °C, and then stored at 4 °C. JellaGel™ was diluted to 32 μg/mL by adding 85 μL of a 3 g/L stock to 7.9 mL of cell culture grade water. 100 μL of the obtained solution was added to each well of a TPP 96 well culture plate and incubated for 24 h at 4 °C. After incubation JellaGel™ was removed and the plate was allowed to air dry in a sterile safety cabinet for 1 h. The wells were rinsed with the cell culture media followed by adding cells at the desired density. To prepare JellaGel™ with laminin at 80:20%, JellaGel™ was diluted to 32 μg/mL by adding 85 μL of 3 g/L stock to 7.9 mL of cell culture grade water. Laminin 2020 was diluted to 10 μg/mL in PBS. 200 μL of the solution was then added to 800 μL of JellaGel™ and mixed by repeat pipetting. 100 μL of the obtained 80:20 solution was added to each well of a TPP 96 well culture plate and incubated for 24 h at 4 °C. The wells were rinsed with the cell culture media followed by adding cells at the desired density.

3.11. Neural cell culture

Astrocytes were thawed (37 °C) and transferred to 15-mL centrifuge tubes. 10 mL of astrocyte maturation media (AMM) was added to the cells, which were then spun down (5 min, 300×*g*), re-suspended in 1 mL of AMM, and counted. The cells were then re-suspended at 3.3×10^6/mL or 1.65×10^6/mL for 1 and 0.5×10^5/cm^2, respectively. 100 μL of the obtained suspension was plated onto 96 well plates coated with JellaGel™ or Matrigel™. The astrocytes were cultured over 1 or 7 days before adding neurons, changing AMM every other day. On day 2, one half of the astrocytes (50%) were treated with an astrocyte mitomix (AMM, 10 μM uridine, 10 μM 5-fluro-2-deoxyuridine) to arrest proliferation, and the other half with AMM.

Neurons were thawed (37 °C) and transferred to 15-mL centrifuge tubes 2.10 mL of neuronal maturation media (NMM) was added to the cells, which were then spun down (3 min, 300×*g*) and the cells were re-suspended in 1 mL of cortical maturation media (CMM) and counted. The cells were then re-suspended at 6.6×10^6/mL and 100 μL of the obtained suspension was platted onto the wells containing astrocytes (7 days and 1 day). 100 μL of CMM was added to the wells with no neurons added. The cells were cultured for another 7 days (unless stated otherwise), with media changed every other day. For fluorescence immunocytochemistry imaging, the co-cultured cells were fixed in 4% paraformaldehyde before imaging. For spontaneous neural activity measurements, the co-cultured cells were treated with 100 μL of Incucyte® Neuroburst Orange Lentivirus regent at different titrations in CMM (15%, 7.5%, 3.75% or 0%). After 24 h the lentivirus solution was removed, and 200 μL of CMM was added. Media changes (50%) were performed every other day. Unless stated otherwise, the cells were treated with a cortical mitomix (CMM, 10 μM uridine, 10 μM 5-fluro-2-deoxyuridine) to arrest proliferation. Incucyte scans for spontaneous neural activity were repeated every 24 h. Images and videos of all the plates were recorded using an IncuCyte® S3 SNA Neuroscience module (Sartorius, Germany) during each phase, with data analysis performed using the manufacturer's software.

3.12. 3D cell culture

Human cervical carcinoma cells (HeLa) were cultured in DMEM with GlutaMAX™ and with heat inactivated fetal bovine serum (FBS; 10%, v/v). Human osteosarcoma cells (MG-63) were cultured in Minimal Essential Eagle's Medium (MEM) with GlutaMAX™, 1% non-essential amino acids supplemented with heat inactivated FBS (10%, v/v). Human breast cancer cells (MCF7) were cultured in Minimal Essential Eagle's Medium (MEM) with GlutaMAX™ and heat inactivated FBS (10%, v/v). Human dermal fibroblasts (Invitrogen, UK) were maintained in Medium 106 supplemented with low serum growth supplement (2%, v/v). Human osteoblasts (PromoCell, Germany) were maintained in osteoblast growth media supplemented with FBS (10%, v/v). Human mesenchymal stem cells (Sigma Aldrich, UK) were maintained in MesenPRO RS™ medium comprising MesenPRO RS™ Basal medium and MesenPRO RS™ growth supplement (ThermoFisher, UK). All cell lines were maintained at 37 °C under a humidified atmosphere of

5% CO_2. At 70–80% confluency, cells were washed with PBS to remove the unattached cells. The adhered cells were trypsinized (TrypLE™ Express) and then treated using trypsin neutralizer (all from Gibco, UK). The harvested cells were centrifuged at 150×*g* for 5 min, and the supernatant was discarded. Cells were then seeded into JellaGel™ and Matrigel™ at the density of 4×10^5 per mL. Spheroid formation using MCF7 cells was probed using a range of cell densities ($1–5 \times 10^5$ per mL).

3.13. 3D cell-matrix preparation

JellaGel™ solutions were prepared as per the manufacturer's protocol (Jellagen, UK). The solutions were added to the centrifuged cell mass, pipetted to evenly distribute the cells, and left at room temperature for 30 min. Cell-specific cultures (as above) were added to the resulting cell-matrix ensembles, which were then incubated at 37 °C, 5% over set periods of time, i.e., 1, 3, 7 days. Ibidi chambers were used for imaging and PrestoBlue® analysis.

Growth factor reduced Matrigel™ solutions were prepared as per the manufacturer's protocol (Corning, UK). Frozen preparation (as supplied) was thawed overnight in the fridge and prior to the cell encapsulation. All pipette tips, Eppendorf tubes and cell suspensions were placed on ice. The cells were evenly mixed in the resulting ice-cold solution and dispensed into culture dishes, followed by incubation at 37 °C, 5% CO_2. Cell-specific cultures as described above were then added to the ensemble. Ibidi chambers were used for imaging and used for PrestoBlue® analysis.

3.14. Fluorescence imaging

For live-dead cell imaging, matrix encapsulated cells were stained using calcein AM (CAM) and propidium iodide (PI) (both from ThermoFisher, UK). Calcein AM is a non-fluorescent molecule that permeates live cells. The hydrolysis of CAM by intracellular esterases produces calcein – a hydrophilic, strongly fluorescent compound that is retained in the cytoplasm. PI is a DNA counterstain that permeates dead cells.

For fixed cell imaging, actin staining was performed with Alexa Fluor® 488 conjugated to phalloidin (Life Technologies, UK) at set incubation time points. The cells were rinsed with PBS (pH 7.4), fixed in 10% neutral buffered formalin solution (Sigma Aldrich, UK) for 15 min at room temperature, washed with PBS and permeabilised using 0.1% Triton- X 100 in PBS. Cells were then extensively washed in PBS and incubated for 30 min at room temperature with Alexa Fluor 488 conjugated *phalloidin* in PBS. After washing with PBS, nuclei were stained with Hoechst 33342 (ThermoFisher, UK). Click-iT 5-ethynyl-2′-deoxyuridine (EdU) Cell Proliferation Kit (ThermoFisher, UK), which is optimized for fluorescence microscopy applications was used to stain proliferating cells. This assay uses a modified thymidine analogue EdU to incorporate into newly synthesized DNA, which is then fluorescently labelled with Alexa Fluor® 488 dye via a specific click reaction.

Cells stained at set time points (e.g., 1, 3, 5, 7 days ±1 day) were imaged using an inverted confocal laser scanning microscope (FV-1000 IX81, Olympus) with 405 nm LD and 488 nm solid state laser with output laser class 2 with 10-60x objective lenses, NA 0.4–1.4. Images were processed using the proprietary software.

3.15. Cell viability and proliferation assays

PrestoBlue® HT reagent (ThermoFisher, UK) was used to measure proliferation at set incubation time points. The reagent was mixed with the cell specific culture media in a 1:10 ratio, and 200 μL of the resulting solution was then dispensed into the wells containing the cell-laden hydrogels in 96 well plates. Following incubations (1 h, 37 °C) 100-μL aliquots were taken out and placed into 96 well plates. Fluorescence was then measured with a microplate reader (BMG, Labtech) using 544-nm excitation and 590-nm emission filters. The proliferation rates are expressed as the percentage of viable cell count in the total cell count. Total number of cells on day 7 was taken as 100%.

Author contributions

Nilofar Faruqui: Conceptualization, Methodology, Validation, Investigation, Writing original draft. **David S Williams**: Conceptualization, Methodology, Investigation, Writing - review & editing. **Andrea Briones, Ibolya E Kepiro, Jascindra Ravi, and Tristan O C Kwan**: Validation, Methodology, Investigation, Writing - review & editing. **Andrew Mearns-Spragg and Maxim G Ryadnov**: Conceptualization, Supervision, Funding acquisition, Writing original draft.

Declaration of competing interest

The authors declare the following financial interests/personal relationships which may be considered as potential competing interests:. Andrew Mearns Spragg has patent #20230148082 pending to Jellagen Limited.

Data availability

Data will be made available on request.

Acknowledgements

We acknowledge funding from the UK's Department for Business, Energy and Industrial Strategy and from Innovate UK (Analysis for Innovators Programme). We thank Censo Biotechnologies for help with neural cell culture and measurements, and Cambridge Advanced Imaging Centre for help with electron microscopy measurements.

Appendix A. Supplementary data

Supplementary data to this article can be found online at https://doi.org/10.1016/j.mtbio.2023.100786.

References

[1] J.K. Mouw, G. Ou, V.M. Weaver, Extracellular matrix assembly: a multiscale deconstruction, Nat. Rev. Mol. Cell Biol. 15 (2014) 771–785.
[2] A.P. McGuigan, S. Javaherian, Tissue patterning: translating design principles from in vivo to in vitro, Annu. Rev. Biomed. Eng. 18 (2016) 1–24.
[3] D.E. Discher, D.J. Mooney, P.W. Zandstra, Growth factors, matrices, and forces combine and control stem cells, Science 324 (2009) 1673–1677.
[4] J. Winkler, A. Abisoye-Ogunniyan, K.J. Metcalf, Z. Werb, Concepts of extracellular matrix remodelling in tumour progression and metastasis, Nat. Commun. 11 (2020) 5120.
[5] D. Seliktar, Designing cell-compatible hydrogels for biomedical applications, Science 336 (2012) 1124–1128.
[6] H. Clevers, Modeling development and disease with organoids, Cell 165 (2016) 1586–1597.
[7] G.G. Giobbe, C. Crowley, C. Luni, S. Campinoti, M. Khedr, K. Kretzschmar, M.M. De Santis, E. Zambaiti, F. Michielin, L. Meran, et al., Extracellular matrix hydrogel derived from decellularized tissues enables endodermal organoid culture, Nat. Commun. 10 (2019) 5658.
[8] S. Kim, S. Min, Y.S. Choi, S.H. Jo, J.H. Jung, K. Han, J. Kim, S. An, Y.W. Ji, Y. G. Kim, S.W. Cho, Tissue extracellular matrix hydrogels as alternatives to Matrigel for culturing gastrointestinal organoids, Nat. Commun. 13 (2022) 1692.
[9] H.K. Kleinman, G.R. Martin, Matrigel: basement membrane matrix with biological activity, Semin. Cancer Biol. 15 (2005) 378–386.
[10] N. Gjorevski, N. Sachs, A. Manfrin, S. Giger, M.E. Bragina, P. Ordóñez-Morán, H. Clevers, M.P. Lutolf, Designer matrices for intestinal stem cell and organoid culture, Nature 539 (2016) 560–564.
[11] O. Chaudhuri, J. Cooper-White, P.A. Janmey, D.J. Mooney, V.B. Shenoy, Effects of extracellular matrix viscoelasticity on cellular behaviour, Nature 584 (2020) 535–546.
[12] R. Langer, D. Tirrell, Designing materials for biology and medicine, Nature 428 (2004) 487–492.
[13] C.M. Rubert Pérez, N. Stephanopoulos, S. Sur, S.S. Lee, C. Newcomb, S.I. Stupp, The powerful functions of peptide-based bioactive matrices for regenerative medicine, Ann. Biomed. Eng. 43 (2015) 501–514.

[14] A.P. Nowak, V. Breedveld, L. Pakstis, B. Ozbas, D.J. Pine, D. Pochan, T.J. Deming, Rapidly recovering hydrogel scaffolds from self-assembling diblock copolypeptide amphiphiles, Nature 417 (2002) 424–428.

[15] G.A. Silva, C. Czeisler, K.L. Niece, E. Beniash, D.A. Harrington, J.A. Kessler, S. I. Stupp, Selective differentiation of neural progenitor cells by high-epitope density nanofibers, Science 303 (2004) 1352–1355.

[16] A. Bella, S. Ray, M. Shaw, M.G. Ryadnov, Arbitrary self-assembly of peptide extracellular microscopic matrices, Angew. Chem., Int. Ed. Engl. 51 (2012) 428–431.

[17] V.A. Kumar, N.L. Taylor, S. Shi, B.K. Wang, A.A. Jalan, M.K. Kang, N. C. Wickremasinghe, J.D. Hartgerink, Highly angiogenic peptide nanofibers, ACS Nano 9 (2015) 860–868.

[18] A.J. Engler, S. Sen, H.L. Sweeney, D.E. Discher, Matrix elasticity directs stem cell lineage specification, Cell 126 (2006) 677–689.

[19] D.E. Discher, P. Janmey, Y.L. Wang, Tissue cells feel and respond to the stiffness of their substrate, Science 310 (2005) 1139–1143.

[20] J.G. Miller, S.A. Hughes, C. Modlin, V.P. Conticello, Structures of synthetic helical filaments and tubes based on peptide and peptido-mimetic polymers, Q. Rev. Biophys. 21 (2022) 1–103.

[21] S. Rele, Y. Song, R.P. Apkarian, Z. Qu, V.P. Conticello, E.L. Chaikof, D-periodic collagen-mimetic microfibers, J. Am. Chem. Soc. 129 (2007) 14780–14787.

[22] L.E. O'Leary, J.A. Fallas, J.D. Hartgerink, Positive and negative design leads to compositional control in AAB collagen heterotrimers, J. Am. Chem. Soc. 133 (2011) 5432–5443.

[23] D. Papapostolou, A.M. Smith, E.D. Atkins, S.J. Oliver, M.G. Ryadnov, L.C. Serpell, D.N. Woolfson, Engineering nanoscale order into a designed protein fiber, Proc. Natl. Acad. Sci. USA 104 (2007) 10853–10858.

[24] D. Wu, N. Sinha, J. Lee, B.P. Sutherland, N.I. Halaszynski, Y. Tian, J. Caplan, H. V. Zhang, J.G. Saven, C.J. Kloxin, D.J. Pochan, Polymers with controlled assembly and rigidity made with click-functional peptide bundles, Nature 574 (2019) 658–662.

[25] S.R. Inamdar, D.P. Knight, N.J. Terrill, A. Karunaratne, F. Cacho-Nerin, M. M. Knight, H.S. Gupta, The secret life of collagen: temporal changes in nanoscale fibrillar pre-strain and molecular organization during physiological loading of cartilage, ACS Nano 11 (2017) 9728–9737.

[26] D.F. Holmes, C.J. Gilpin, C. Baldock, U. Ziese, A.J. Koster, K.E. Kadler, Corneal collagen fibril structure in three dimensions: structural insights into fibril assembly, mechanical properties, and tissue organization, Proc. Natl. Acad. Sci. USA 98 (2001) 7307–7312.

[27] D.F. Holmes, Y. Lu, T. Starborg, K.E. Kadler, Collagen fibril assembly and function, Curr. Top. Dev. Biol. 130 (2018) 107–142.

[28] T.D. Clemons, S.I. Stupp, Design of materials with supramolecular polymers, Prog. Polym. Sci. 111 (2020), 101310.

[29] S. Lou, X. Wang, Z. Yu, L. Shi, Peptide tectonics: encoded structural complementarity dictates programmable self-assembly, Adv. Sci. 6 (2019), 1802043.

[30] M.G. Ryadnov, D.N. Woolfson, Engineering the morphology of a self-assembling protein fibre, Nat. Mater. 2 (2003) 329–332.

[31] M.G. Ryadnov, D.N. Woolfson, MaP peptides: programming the self-assembly of peptide-based mesoscopic matrices, J. Am. Chem. Soc. 127 (2005) 12407–12415.

[32] N. Faruqui, A. Bella, J. Ravi, S. Ray, B. Lamarre, M.G. Ryadnov, Differentially instructive extracellular protein micro-nets, J. Am. Chem. Soc. 136 (2014) 7889–7898.

[33] S. Ricard-Blum, The collagen family, Cold Spring Harbor Perspect. Biol. 3 (2011) a004978.

[34] A. Pertsemlidis, J.W. Fondon, Having a BLAST with bioinformatics (and avoiding BLASTphemy), Genome Biol. 2 (2001) 1–10.

[35] T.-F. Chan, A. Poon, A. Basu, N.R. Addleman, J. Chen, A. Phong, P.H. Byers, T. E. Klein, P.-Y. Kwok, Natural variation in four human collagen genes across an ethnically diverse population, Genomics 91 (2008) 307–314.

[36] A.J. Bowen, D.C. Ekbom, D. Hunter, S. Voss, K. Bartemes, A. Mearns-Spragg, M. S. Oldenburg, S. San-Marina, Larynx proteomics after jellyfish collagen IL: increased ECM/collagen and suppressed inflammation, Laryngoscope Investig. Otolaryngol. 7 (2022) 1513–1520.

[37] J. Zhao, W. Yu, Q. Zhang, X. Li, Y. Huang, S. Zhao, T. Li, S. Liu, Y. Li, H. Shan, Structural and biofunctional evaluation of decellularized jellyfish matrices, J. Mater. Chem. B 11 (2023) 3740–3751.

[38] I. Flaig, M. Radenković, S. Najman, A. Pröhl, O. Jung, M. Barbeck, *In vivo* analysis of the biocompatibility and immune response of jellyfish collagen scaffolds and its suitability for bone regeneration, Int. J. Mol. Sci. 21 (2020) 4518.

[39] F. Paradiso, J. Fitzgerald, S. Yao, F. Barry, F. Taraballi, D. Gonzalez, R.S. Conlan, L. Francis, Marine collagen substrates for 2D and 3D ovarian cancer cell systems, Front. Bioeng. Biotechnol. 7 (2019) 343.

[40] E. Song, S. Yeon Kim, T. Chun, H.J. Byun, Y.M. Lee, Collagen Scaffolds derived from a marine source and their biocompatibilty, Biomaterials 27 (2006) 2951–2961.

[41] Z. Ahmed, L.C. Powell, N. Matin, A. Mearns-Spragg, C.A. Thornton, I.M. Khan, L. W. Francis, Jellyfish collagen: a biocompatible collagen source for 3D scaffold fabrication and enhanced chondrogenicity, Mar. Drugs 19 (2021) 405.

[42] X. Cheng, Z. Shao, C. Li, L. Yu, M.A. Raja, C. Liu, Isolation, characterization and evaluation of collagen from jellyfish Rhopilema esculentum Kishinouye for use in hemostatic applications, PLoS One 12 (2017), e0169731.

[43] S. Addad, J.Y. Exposito, C. Faye, S. Ricard-Blum, C. Lethias, Isolation, characterization and biological evaluation of jellyfish collagen for use in biomedical applications, Mar. Drugs 9 (2011) 967–983.

[44] B. Hoyer, A. Bernhardt, A. Lode, S. Heinemann, J. Sewing, M. Klinger, H. Notbohm, M. Gelinsky, Jellyfish collagen scaffolds for cartilage tissue engineering, Acta Biomater. 10 (2014) 883–892.

[45] J.P. Widdowson, A.J. Picton, V. Vince, C.J. Wright, A. Mearns-Spragg, In vivo comparison of jellyfish and BCTI sponges as prototype medical devices, J. Biomed. Mater. Res. B Appl. Biomater. 106 (2018) 1524–1533.

[46] W. Pustlauk, B. Paul, S. Brueggemeier, M. Gelinsky, A. Bernhardt, Modulation of chondrogenic differentiation of human mesenchymal stem cells in jellyfish collagen scaffolds by cell density and culture medium, J. Tissue Eng. Regen. Med. 11 (2017) 1710–1722.

[47] A. Higuchi, Q.D. Ling, Y. Chang, S.T. Hsu, A. Umezawa, Physical cues of biomaterials guide stem cell differentiation fate, Chem. Rev. 113 (2013) 3297–3328.

[48] Y. Li, et al., Engineering cell alignment in vitro, Biotechnol. Adv. 32 (2014) 347–365.

[49] G.S. Hussey, J.L. Dziki, S. Badylak, Extracellular matrix-based materials for regenerative medicine, Nat. Rev. Mater. 3 (2018) 159–173.

[50] J.P.R.O. Orgel, T.C. Irving, A. Miller, T.J. Wess, Microfibrillar structure of type I collagen in situ, Proc. Natl. Acad. Sci. USA 103 (2006) 9001–9005.

[51] M.G. Ryadnov, D.N. Woolfson, Self-assembled templates for polypeptide synthesis, J. Am. Chem. Soc. 129 (2007) 14074–14081.

[52] M.G. Ryadnov, A. Bella, S. Timson, D.N. Woolfson, Modular design of peptide fibrillar nano- to microstructures, J. Am. Chem. Soc. 131 (2009) 13240–13241.

[53] D.F. Holmes, H.K. Graham, J.A. Trotter, K.E. Kadler, STEM/TEM studies of collagen fibril assembly, Micron 32 (2001) 273–285.

[54] R.W. Woody, Circular dichroism spectrum of peptides in the poly(Pro)II conformation, J. Am. Chem. Soc. 131 (2009) 8234–8245.

[55] A.L. Rucker, T.P. Creamer, Polyproline II helical structure in protein unfolded states: lysine peptides revisited, Protein Sci. 11 (2002) 980–985.

[56] M.R. Hicks, J. Kowałski, A. Rodger, LD spectroscopy of natural and synthetic biomaterials, Chem. Soc. Rev. 39 (2010) 3380–3393.

[57] T.R. Dafforn, J. Rajendra, D.J. Halsall, L.C. Serpell, A. Rodger, Protein fiber linear dichroism for structure determination and kinetics in a low-volume, low-wavelength Couette flow cell, Biophys. J. 86 (2004) 404–410.

[58] L. Bozec, M. Odlyha, Thermal denaturation studies of collagen by microthermal analysis and atomic force microscopy, Biophys. J. 101 (2011) 228–236.

[59] M. Gauza-Włodarczyk, L. Kubisz, S. Mielcarek, D. Włodarczyk, Comparison of thermal properties of fish collagen and bovine collagen in the temperature range 298-670K, Mater. Sci. Eng., C 80 (2017) 468–471.

[60] M. Fields, N. Spencer, J. Dudhia, P.F. McMillan, Structural changes in cartilage and collagen studied by high temperature Raman spectroscopy, Biopolymers 107 (2017), e23017.

[61] P.E. McClain, E.R. Wiley, Differential scanning calorimeter studies of the thermal transitions of collagen. Implications on structure and stability, J. Biol. Chem. 247 (1972) 692–697.

[62] A. Miki, S. Inaba, T. Baba, K. Kihira, H. Fukada, M. Oda, Structural and physical properties of collagen extracted from moon jellyfish under neutral pH conditions, Biosci. Biotechnol. Biochem. 79 (2015) 1603–1607.

[63] J.A. Cañas, J.M. Rodrigo-Muñoz, S.H. Rondon-Cepeda, C. Bordehore, M. Fernández-Nieto, V. Del Pozo, Jellyfish collagen: a new allergen in the beach, Ann. Allergy Asthma Immunol. 120 (2018) 430–431.

[64] M.R. Cohen, A. Kohn, Measuring and interpreting neuronal correlations, Nat. Neurosci. 14 (2011) 811–819.

[65] D.S. Reich, F. Mechler, J.D. Victor, Independent and redundant information in nearby cortical neurons, Science 294 (2001) 2566, 2558.

[66] C. Chang, J. Yan, Z. Yao, C. Zhang, X. Li, H.Q. Mao, Effects of mesenchymal stem cell-derived paracrine signals and their delivery strategies, Adv. Healthcare Mater. 10 (2021), e2001689.

[67] J. Zonderland, L. Moroni, Steering cell behavior through mechanobiology in 3D: a regenerative medicine perspective, Biomaterials 268 (2021), 120572.

[68] R. Poincloux, O. Collin, F. Lizárraga, M. Romao, M. Debray, M. Piel, P. Chavrier, Contractility of the cell rear drives invasion of breast tumor cells in 3D Matrigel, Proc. Natl. Acad. Sci. U.S.A. 108 (2011) 1943–1948.

[69] K. Wolf, I. Mazo, H. Leung, K. Engelke, U.H. von Andrian, E.I. Deryugina, A. Y. Strongin, E.B. Bröcker, P. Friedl, Compensation mechanism in tumor cell migration: mesenchymal-amoeboid transition after blocking of pericellular proteolysis, J. Cell Biol. 160 (2003) 267–277.

[70] M.A. Lancaster, J.A. Knobloch, Organogenesis in a dish: modeling development and disease using organoid technologies, Science 345 (2014), 1247125.

[71] W. Kim, Y. Gwon, S. Park, H. Kim, J. Kim, Therapeutic strategies of three-dimensional stem cell spheroids and organoids for tissue repair and regeneration, Bioact. Mater. 19 (2022) 50–74.

[72] G. Benton, G. DeGray, H.K. Kleinman, J. George, I. Arnaoutova, *In vitro* microtumors provide a physiologically predictive tool for breast cancer therapeutic screening, PLoS One 10 (2015), e0123312.

[73] Y. Li, E. Kumacheva, Hydrogel microenvironments for cancer spheroid growth and drug screening, Sci. Adv. 4 (2018), eaas8998.

[74] T.A. Phillips, V. Caprettini, N. Aggarwal, S. Marcotti, R. Tetley, Y. Mao, T. Shaw, C. Chiappini, M. Parsons, S. Cox, A method for reproducible high-resolution imaging of 3D cancer cell spheroids, J. Microsc. 291 (2023) 30–42.

[75] S.S. Nazari, Generation of 3D tumor spheroids with encapsulating basement membranes for invasion studies, Curr. Protoc. Cell Biol. 87 (2020) e105.

[76] E. Entcheva, H. Bien, L. Yin, C.-Y. Chung, M. Farrell, Y. Kostov, Functional cardiac cell constructs on cellulose-based scaffolding, Biomaterials 25 (2004) 5753–5762.

[77] C. Lugassy, S. Zadran, L. Laurent Bentolila, M. Wadehra, R. Prakash, S. T. Carmichael, H. Kleinman, B. Péault, L. Larue, R.L. Barnhill, Angiotropism,

pericytic mimicry and extravascular migratory metastasis in melanoma: an alternative to Intravascular cancer dissemination, Cancer Microenviron 6 (2013) 19–29.
[78] A. Passaniti, H.K. Kleinman, G. Martin, R. Matrigel, history/background, uses, and future applications, J. Cell Commun. Signal. 16 (2022) 621–626.
[79] S.R. Caliari, J.A. Burdick, A practical guide to hydrogels for cell culture, Nat. Methods 13 (2016) 405–414.
[80] M. Meyer, Processing of collagen based biomaterials and the resulting materials properties, Biomed. Eng. Online 18 (2019) 24.